SUBSONIC ORGANIC VAPOR FLOW PAST A CIRCULAR CYLINDER

Paola Cinnella[1]*, Camille Matar[1], Xavier Gloerfelt[2], Felix Reinker[3], Stefan aus der Wiesche[3]

[1]Sorbonne Université, Institut Jean Le Rond D'Alembert, Paris, France

[2]Arts et Métiers Institut of Technology, Laboratoire DynFluid, Paris, France

[3]Muenster University of Applied Sciences, Department of Mechanical Engineering, Steinfurt, Germany

*Corresponding Author: paola.cinnella@sorbonne-universite.fr

ABSTRACT

Numerical simulations of subsonic flows past a circular cylinder of an organic fluid (Novec^{TM} 649) at various operating conditions are reported in the aim of complementing recent experimental investigations conducted in the CLOWT wind tunnel at Muenster University of Applied Sciences. The configuration is representative of a rotatable Pitot cylinder probe in the crossflow of an organic vapor stream. The present results, obtained by solving the steady Reynolds-Averaged Navier-Stokes equations supplemented by the one-equation model of Spalart and Allmaras, are in reasonably good agreement with the experiments. The results show that non-ideal gas effects play a minor role in the range of conditions considered in the experiments, and that discrepancies with respect to air flow at the same Mach and Reynolds number are an effect of the different isentropic exponents.

1 INTRODUCTION

The compressible flow of a perfect gas past a circular cylinder has been investigated intensively and numerous papers are now available in the open literature dealing with this canonical problem (see, e.g., Zdravkovich, 2003). The circular cylinder configuration is attractive for scientists because important fundamental flow phenomena like boundary layer transition and vortex shedding can be studied, and it is an obvious starting point for many technical applications including the impact of Pitot probe stems and blockage corrections in experimental studies. Ackerman *et al*. (2008) investigated in detail the base pressure behaviour of a circular cylinder in the high subsonic crossflow of air as an idealized model for the study of trailing edge losses of turbine blades, for which the base pressure is a crucial parameter (Denton, 1993). However, data on cylinder wall pressure distribution and drag in the high subsonic flow regime in streams of non-ideal gases are essentially missing in literature so far. Non-ideal compressible flows of molecularly complex vapours have become an emerging topic for diverse industrial applications such as ORC power systems. Recently, Reinker *et al.* (2021) measured various flow properties around cylinders in the crossflow of an organic vapor (Novec™ 649) and of air over the low subsonic ($M < 0.4$) and mid to high subsonic ($0.4 < M < 0.8$) speed range in a continuously running pressurized closed-loop wind tunnel test facility, CLOWT (Closed Loop Organic Wind Tunnel, Reinker et al., 2018). The study aimed at investigating the performance of rotatable cylinder Pitot probes for total pressure measurements in Organic Rankine Cycle (ORC) turbines. Time-averaged pressure measurements gave information on surface pressure distributions, and the corresponding drag and base pressure drag coefficients were obtained. The results were compared to data available in the literature for air flows and changes in surface pressure distribution at higher subsonic velocities were identified. The new results for the organic vapor flow were in reasonable agreement with literature data obtained for air, with some deviations attributed to Reynolds number effects or experimental uncertainty range. The deviations between the organic vapor flow and literature data were of the same order as the

scattering of the literature data, leading to the conclusion that non-ideal gas effects were of minor importance for the overall flow behaviour at the considered Mach number range. It must be noted that, due to wind tunnel constraints and to the high density of the working fluid, a very small cylinder with a diameter of 0.5 cm was tested. At such small dimensions, the geometry exhibited significant relative roughness, which had an impact on the transition point in the very sensitive range of considered Reynolds numbers, encompassing the drag crisis. Therefore, numerical simulations may represent a very useful complement to experiments to quantify to which amount the measured discrepancies between air and organic fluid flows are to be attributed to non-ideal gas effects or to experimental uncertainties.

In this contribution, numerical simulations of the cylinder flow are carried out at various Mach numbers in the range [0.1,0.65] using standard air or Novec™ 649. For the latter, various freestream thermodynamic states are considered, ranging from mildly non-ideal to strongly non-ideal conditions.

2 NUMERICAL METHOD

The Reynolds-Averaged Navier-Stokes (RANS) equations are solved by using an in-house structured finite volume code used in previous studies of non-ideal gas flows by the first author (Cinnella and Congedo, 2005). The inviscid fluxes are discretized using a nominally third-order accurate central scheme with weighted coefficients to account for irregular mesh spacing (Rezgui et al., 2001). A five-points-per-direction second-order approximation is used for the viscous fluxes and the solution is advanced in time using a four-stage Runge-Kutta scheme supplemented with implicit residual smoothing at each stage, to enable the use of large time steps and speed-up convergence to a steady state solution. The code is equipped with various real-gas equations of state. For the present calculations we adopted the Peng-Robinson-Stryjek-Vera (1986) thermal equation of state, along with a simple power law modeling the dependency of the dilute-gas constant-volume heat capacity on the temperature (see, e.g. Congedo *et al*., 2011, for an assessment of the accuracy of the PRSV equation of state for selected heavy organic fluids). The molecular viscosity and thermal conductivity are described using the Chung et al. (1988) models. The Spalart-Allmaras turbulence model is used to account for turbulent stresses.

Table 1: Properties of Novec™ 649.

Critical temperature	Critical pressure	Acentric factor	Molar Weight	Critical Heat capacity
441.81 K	1.869 MPa	0.471	316 g/mol	975.96 J $kg^{-1}K^{-1}$

The solution was computed in the rectangular domain $[-30,40] \times [-20,20]$, where all length scales are made nondimensional with the cylinder diameter. The domain was discretized with meshes composed of five structured blocks: a 0-shaped block around the cylinder and four H-shaped blocks. The first grid (called grid A) has a total number of mesh cells equal to 25888, the cylinder wall being discretized by 80 cells and the height of the first cell close to the wall being such that $y^+ \approx 2$ in average. Three other grids, labelled B, C and D, respectively, were considered. Grid B was obtained by doubling the number of mesh points in the wall normal direction (leading to $y^+ \approx 1$) only; grid C was obtained by doubling the number of cells in the tangential direction with respect to grid A (in which case $y^+ \approx 2$ and the cylinder is discretized by 160 cells); finally, grid D was refined in both directions ($y^+ \approx 1$ and 160 points along the cylinder). The results are reported in Figure 1 for air flow at a freestream Mach number of 0.6 and Reynolds number equal to 6.1×10^5. Results for grids A, B and D are very similar, with maximum differences of less than 5% at the suction peak, showing that the results a nearly mesh independent. A steady-state solution could not be achieved for grid C. For the parametric study presented in the following we retained grid A.

For all cases discussed in Section 4, the solution residuals were reduced by more than five orders of magnitude with respect to the first iteration.

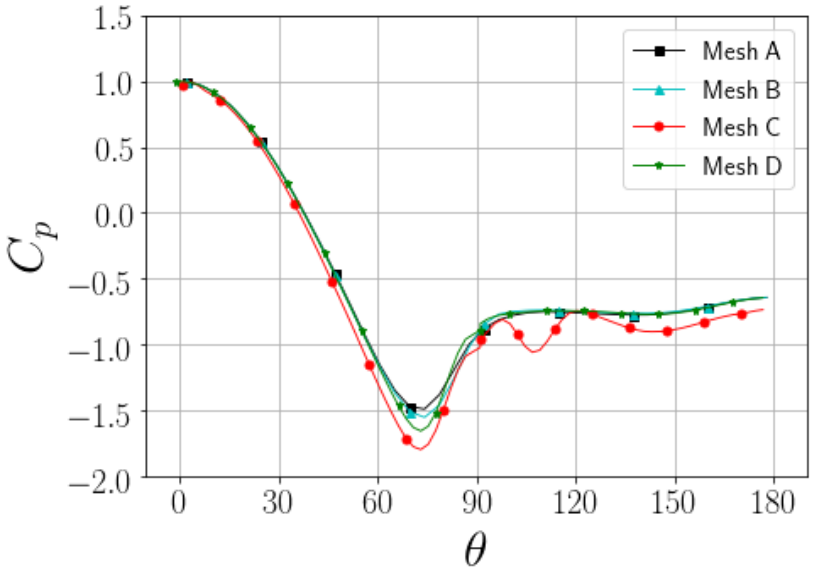

Figure 1: Mesh convergence study. Computed distribution of the wall pressure coefficient versus the azimuthal coordinate θ for air at Mach 0.6 and Re 6.1×10^5 (b).

Table 2: Freestream conditions of the cylinder simulations.

Fluid	Reduced pressure p/p_c	Reduced temperature T/T_c	Compressibility factor Z	Fundamental derivative Γ	Mach number M_∞	Reynolds number Re_∞
Novec™ 649	0.166	0.0599	0.88	0.938	0.13	10^5
Novec™ 649	0.166	0.0599	0.88	0.938	0.41	4.7×10^5
Novec™ 649	0.166	0.0599	0.88	0.938	0.60	6.1×10^5
Novec™ 649	0.0787	0.0263	0.94	0.983	0.65	3.4×10^5
Novec™ 649	0.553	0.2	0.87	0.852	0.65	3.4×10^5
Novec™ 649	0.884	0.4	0.7	0.732	0.65	3.4×10^5
Novec™ 649	0.948	0.6	0.5	0.578	0.65	3.4×10^5
Air			1	1.2	0.19	1.1×10^5
Air			1	1.2	0.41	4.7×10^5
Air			1	1.2	0.60	6.1×10^5

3 EXPERIMENTAL DATA

The outcomes of the numerical study were compared with available experimental data gathered in experiments utilizing a circular cylinder placed in the test section of a continuously running pressurized closed-loop wind tunnel test facility working with the organic vapor Novec™ 649 (Reinker *et al.*, 2021). Experimental data for air are also available from the same reference. Experimentally, low subsonic (M < 0.4) , mid-subsonic (0.4 < M < 0.6) and high subsonic (M > 0.8) speed ranges were covered. Time-averaged pressure measurements provided information on surface pressure distributions, and the corresponding drag and base pressure drag coefficients were obtained. The variation of drag over the Mach number range was comparable with literature data for ideal-gas compressible flow, including shock-less, intermittent shock wave, and permanent shock-wave regimes. A substantial increase of drag was observed at Mach 0.6 which was attributed to the commencement of transonic regime.

4 RESULTS

Cylinder flows of Novec^{TM} 649 at various freestream Mach and Reynolds numbers (based on cylinder diameter) were simulated in the attempt of reproducing the experimental data. The chosen freestream thermodynamic conditions were also set according to the experiments. Table 2 summarizes all flow conditions considered in the study. For Novec^{TM} 649, we also report numerical results for thermodynamic conditions corresponding to a highly non-ideal thermodynamic behavior, which cannot be attained in the wind tunnel experiments. The location of the most non-ideal freestream conditions in the Clapeyron diagram is reported in Figure 2.

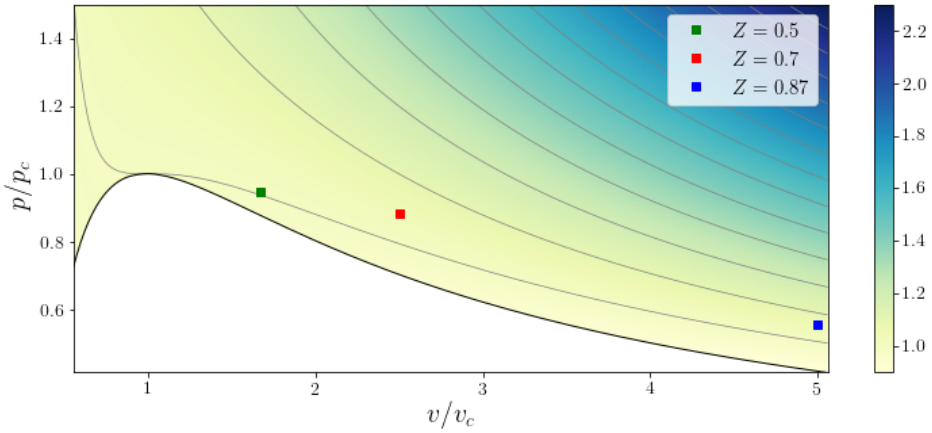

Figure 2: Location of non-ideal freestream thermodynamic conditions in the Clapeyron diagram for Novec^{TM} 649.

In Figure 3 we report the iso-contours of the Mach number around the cylinder along with streamlines highlighting the recirculation region behind the body. As the Mach number increases from 0.13 (nearly incompressible flow) to 0.41 (mid-subsonic conditions), the wave thickness and the size of the recirculation bubble are first decreased. This results from the delay in flow separation under the effect of the favorable pressure acting on the forward-facing part of the cylinder. A local Mach number of approximately 0.7 is reached at the top of the cylinder. When the free-stream Mach number is further increased, the flow exhibits a small supersonic region immediately upstream of the separation point, with local Mach number slightly above 1. The region is possibly terminated by a weak shock, which favors boundary layer separation, and leads to increased wake thickness and recirculation bubble length.

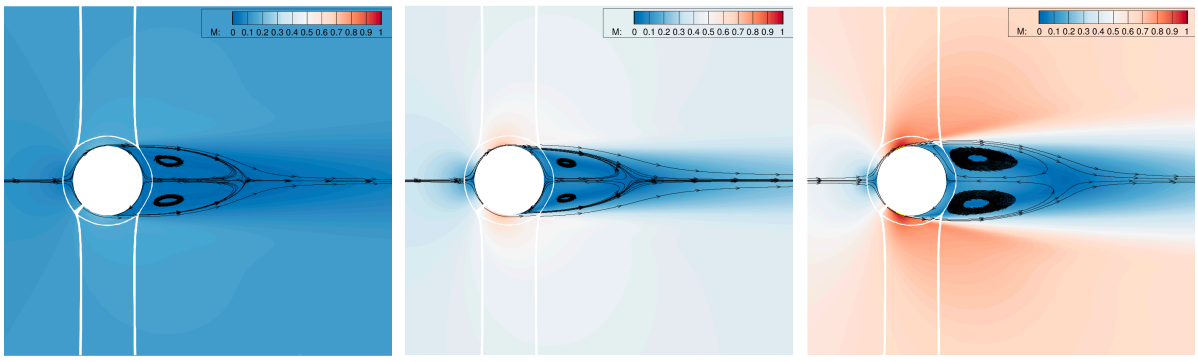

(a) (b) (c)

Figure 3: Iso-contours of the Mach number and flow streamlines for cylinder flows of Novec^{TM} 649 at Mach 0.13 (a), 0.41 (b) and 0.65 (c). In the latter figure, the tiny yellow regions correspond to supersonic flow.

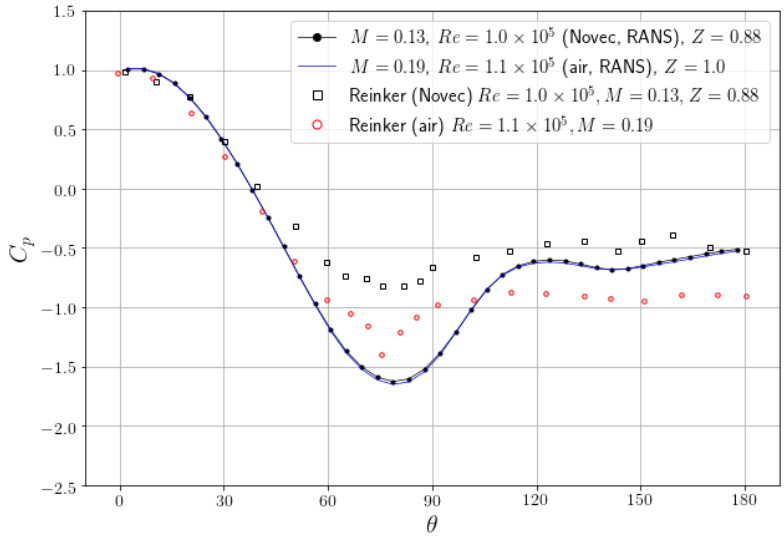

(a)

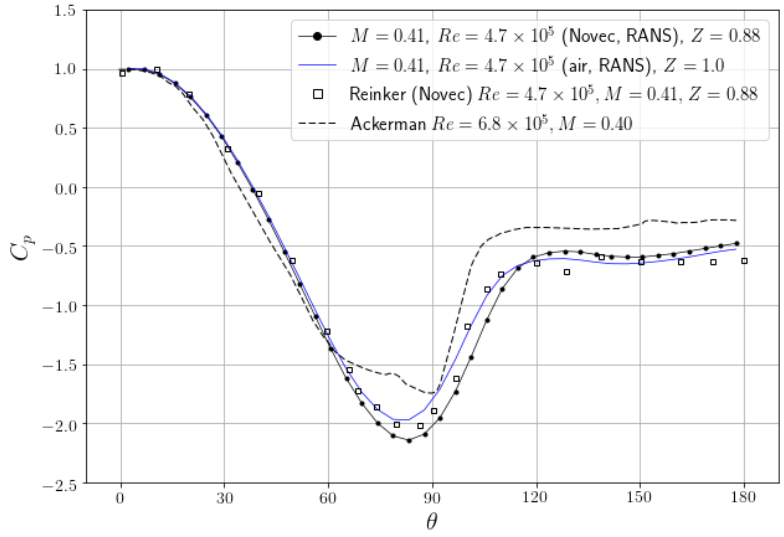

(b)

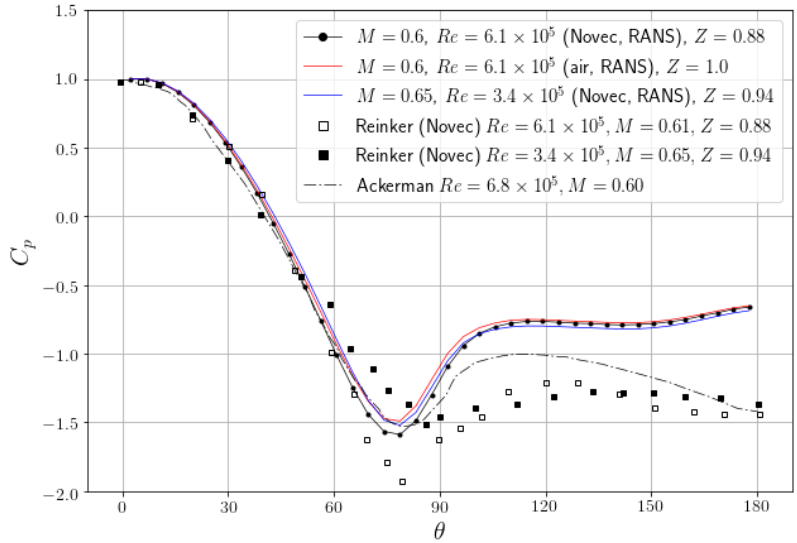

(c)

Figure 4: Pressure coefficient distribution along the cylinder at low-subsonic (top), mid-subsonic (middle) and high-subsonic conditions (bottom). Comparison with experimental data from the CLOWT wind tunnel and from the literature.

Cross comparisons of the present simulations and wind tunnel experiments of Reinker *et al.* (2021) and Ackerman (2008) are reported in Figure 4 for the pressure coefficient $C_p = \frac{p-p_\infty}{p_0-p_\infty}$ along the cylinder at various Mach numbers. The freestream thermodynamic conditions correspond to a weakly non ideal behavior with a compressibility factor $Z \approx 1$. Still, the freestream value of the fundamental derivative of gas dynamics is lower than one, meaning that the speed of sound tends to decrease when the fluid is compressed (dense gas behavior).

At low subsonic conditions (Figure 4(a)), dense gas effects are not expected to play any significant role, and indeed the RANS solutions for Novec^{TM} 649 and air are almost superposed. Minor differences between the two simulations are attributed to the slightly higher Mach number used for air to match the experimental conditions used in CLOWT. The present numerical results are in good agreement with the data of Reinker *et al*. (2021) for air, up to an angle $\theta \approx 60°$. Differences are observed in the region of the suction peak, due to experimental uncertainties as well as to inaccuracies of the steady RANS model in capturing the location of the separation point. In the separated region, the computed C_p is comprised between the two experimental sets from CLOWT and it is somewhat closer to the CLOWT dataset for Novec^{TM} 649. We conclude that this flow regime is particularly challenging for measurements, especially in the separated region, which is extremely sensitive to roughness, small variations of the test conditions, etc…, and that measured differences between air and Novec^{TM} 649 in this regime are mostly a consequence of experimental uncertainties. On the other hand, steady RANS simulations do not provide a sufficiently accurate estimate of the cylinder base pressure.

When the Mach number is increased to 0.41 (Figure 4(b)), a nice agreement is found between the numerical solution and the experiments. For such more compressible conditions, the dense gas exhibits a slightly lower minimum of C_p compared to air, because of its lower speed of sound. Given the weakly non-ideal thermodynamic conditions, the latter is mainly due to the lower isentropic exponent of the molecularly complex dense gas ($\gamma \approx 1.05$ for Novec^{TM} at the considered conditions).

Further increasing the Mach number to 0.6 (Figure 4(c)), deviations between air and Novec^{TM} 649 are still moderate. The present solutions are in reasonably good agreement with experiments from Reinker et al. and Ackerman up to $\theta \approx 70°$. In the suction region the present simulations are still in very good agreement with Ackerman's data up to the angular position $\theta \approx 75°$, while the CLOWT measurements at Mach 0.59 indicate lower values of C_p. In the separated region, the calculations overpredict both sets of experiments. Once again, is likely an effect of turbulence modeling inadequacies and of unsteady flow behavior, not considered in the present steady RANS simulations. Calculations using higher fidelity models (URANS and DDES) are underway to clarify this point. The experimental data for Novec^{TM} 649 at a slightly higher Mach number (0.65) and thermodynamic conditions exhibit substantial deviations with respect to the flow at Mach 0.6, in contrast with the numerical results that are little affected by small changes in these parameters. Such differences are then most likely attributed to experimental uncertainties in test section conditions as well as in cylinder geometry (affecting the separation point location) more than small changes in the freestream conditions.

To further elucidate the role of thermodynamic operating conditions, we carried out numerical simulations by fixing the freestream Mach and Reynolds number and by moving the thermodynamic operating point toward increasingly non ideal conditions. The corresponding results for the pressure coefficient are reported in Figure 5.

For thermodynamic conditions corresponding to weakly non ideal thermodynamic behavior (i.e. $Z = 0.87 \div 0.94$), the numerical results are superposed to within plotting accuracy. Moving to $Z = 0.7$, the minimum of C_p becomes lower as the flow speed of sound decreases. The deviations are more significant for $Z = 0.5$, due to the more and more non-ideal behavior of the gas, yet they remain of the order of 13% in the peak region. It is worth noticing that the fundamental derivative of gas dynamics becomes smaller and smaller as Z is decreased, so that the isentropic exponent is reduced accordingly. This confirms that, in the present range of Mach numbers, the flow around the cylinder is only mildly affected by non-ideal gas effects, and that discrepancies observed in the pressure coefficient distribution with respect to air are mostly explained by the lower isentropic exponent of the dense fluid.

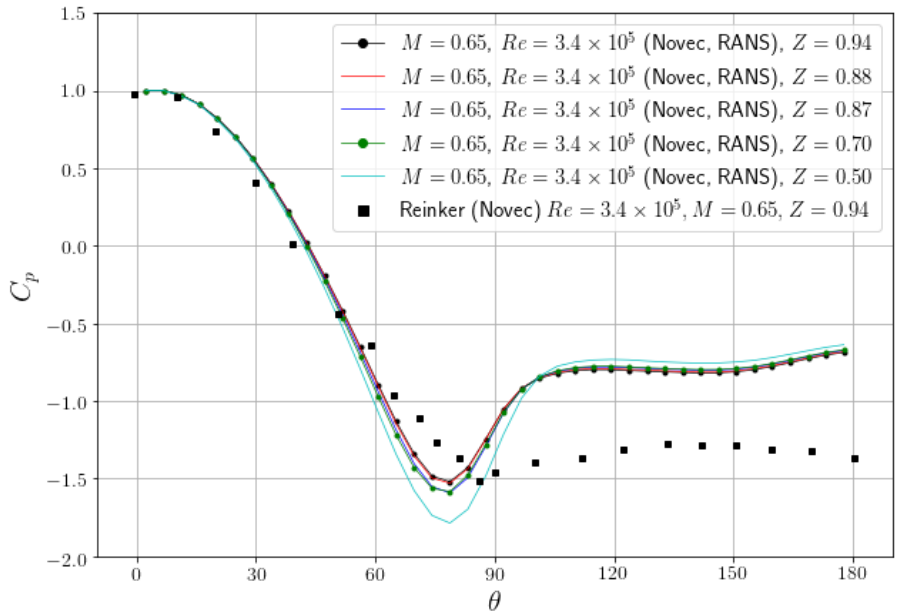

Figure 5: Pressure coefficient distribution along the cylinder for flows at Mach 0.65 and Reynolds 3.4×10^5 at various freestream thermodynamic conditions.

In Table 3 we report the separation angle and the drag coefficient $C_d = \frac{F_x}{\frac{1}{2}\rho_\infty U_\infty^2 D}$ for selected flow conditions. For the latter, experimental data obtained by Reinker *et al*. by integrating the measured pressure coefficient over the cylinder are also reported for comparison. While the experimental data are in good agreement with other data sets in the literature (see Reinker *et al*., 2021), the simulations predict significantly lower values of C_d for most cases, accordingly to the overestimation of the base pressure coefficient observed in Figure 3.

Table 3: Computed drag coefficient, base pressure coefficient, and separation points for cylinders flows at various conditions.

Conditions	**Fluid**	θ_{sep} **(deg)**	C_d**, present**	C_d**, Reinker et al.**
M=0.13, Re=10^5	Novec, Z=0.88	92	0.582	0.88-1.1
M=0.41, Re=4.7×10^5	Novec, Z=0.88	97	0.485	0.6
M=0.6, Re=6.1×10^5	Novec, Z=0.88	83	0.887	0.75-0.82
M=0.65, Re=3.4×10^5	Novec, Z=0.88	83	0.987	1.55
M=0.19, Re=1.1×10^5	Air	92	0.593	1.16
M=0.41, Re=4.7×10^5	Air	92	0.556	-
M=0.6, Re=6.1×10^5	Air	83	0.897	-

Finally, we observe that the separation point varies non monotonically with the Mach number: it initially moves downstream when increasing the flow speed above nearly incompressible conditions, then decreases abruptly above the critical Mach number, due to shock-induced separation. This behavior is in accordance with the observed behavior of the cylinder wake thickness.

5 CONCLUSIONS

- Numerical simulations of low to high subsonic flows of a dense gas, namely Novec^{TM} 649, around a cylinder at Reynolds numbers of the order of 10^5, encompassing the drag crisis, were conducted

using a steady RANS CFD solver, equipped with the Peng-Robinson-Stryjeck-Vera equation of state and the Spalart-Allmaras turbulence model.

- Comparisons between numerical results and experimental data obtained in the dense-gas closed-loop CLOWT wind tunnel could be carried out for the first time.
- Despite inadequacies of steady RANS in capturing the unsteady separated flow behavior in the challenging range of conditions considered in the study, the results were found to be in reasonably good agreement with the experimental measurements obtained by Reinker *et al*. (2021). The steady numerical solution overestimates the base pressure coefficient, leading to an underestimation of the cylinder drag coefficient. This can be improved by adopting higher-fidelity flow models that resolve part of the unsteady flow content. Specifically, unsteady RANS simulations and Detached Eddy Simulations are currently underway and will make the object of a forthcoming communication.
- In turn, the numerical results allowed to assess the experimental data sets, confirming that: 1) the discrepancies observed between experimental data for air and Novec^{TM} 649 at the lowest Mach numbers are an effect of wind-tunnel and geometrical uncertainties and that no substantial differences exist between the two fluids at nearly incompressible conditions; 2) similarly, discrepancies between cylinder flows at slightly different, weakly non-ideal thermodynamic conditions and Mach numbers are also mainly an effect of experimental uncertainties, exacerbated by the transitional Reynolds numbers and cylinder roughness.
- Differences between Novec^{TM} 649 and air flows are observed at the higher Mach numbers, especially if strongly non-ideal conditions are considered. Nevertheless, the deviations remain of minor entity (less than 13% at suction peak), and they can be explained by the lower isentropic coefficient of the dense working fluid more than to non-ideal gas effects.

The present work is part of a larger research program, namely, the REGAL-ORC project funded by the French and German research agencies ANR and DLR. In the frame of this project, high-fidelity measurements and computations of simplified flow configurations representative of ORC turbine blades will be carried out and compared in detail with the aim of better understanding loss mechanisms in ORC turbines.

NOMENCLATURE

C_d	drag coefficient
C_p	pressure coefficient
D	cylinder diameter
M	Mach number
Re	Reynolds number
ρ	fluid density
p	fluid pressure
T	fluid temperature
Γ	fundamental derivative of gas Dynamics

Subscripts

∞	free-stream conditions
0	stagnation conditions

REFERENCES

Ackerman, J.R., Gostelow, J.P., Rona, A., Carscallen, W.E., 2008, Base Pressure Measurements on a Circular Cylinder in Subsonic Cross Flow, AIAA Conference paper, AIAA2008–4305.

Chung, T., Ajlan, M., Lee, L., Starling, K., 1988, Generalized multiparameter correlation for nonpolar and polar fluid transport properties, *Ind. Eng. Chem. Res*., Vol. 27, no. 4: p.671–679.

Cinnella, P., Congedo, P.M., 2005, Numerical Solver for Dense Gas Flows, *AIAA Journal*, Vol. 43, No. 11: p.2457-2464.

Congedo, P. M., Corre, C., Cinnella, P., Numerical investigation of dense-gas effects in turbomachinery, *Computers & Fluids,* Vol. 49, no. 1: p. 290-301.

Denton, J.D., 1993, Loss Mechanisms in Turbomachines, *Journal of Turbomachinery*, vol. 115, no. 3: p. 621-656.

Stryjek, R., Vera, J. H., 1986, PRSV: An improved Peng–Robinson equation of state for pure compounds and mixtures, *The Canadian Journal of Chemical Engineering*, Vol. 64 , no. 2: p. 323–333.

Reinker, F., Kenig, E. Y., aus der Wiesche, S., 2018, CLOWT: A Multifunctional Test Facility for the Investigation of Organic Vapor Flows, Proceedings ASME 2018 5th Joint US-European Fluids Engineering Division Summer Meeting, Montreal, Canada (V002T14A004).

Reinker, F., Wagner, R., Hake, L., aus der Wiesche, S., 2021, High Subsonic Flow of an Organic Vapor past a Circular Cylinder, *Experiments in Fluids*, Vol. 62: p. 54.

Rezgui, A., Cinnella, P., Lerat, A., 2001, Third-order accurate finite volume schemes for Euler computations on curvilinear meshes, *Computers & Fluids*, Vol. 30, no. 7-8: p. 875-901.

Zdravkovich, M.M., 2003, Flow around Circular Cylinders, Chapter 1, p. 566-571. Oxford Science Publisher.

ACKNOWLEDGEMENT

The authors thankfully acknowledge the Agence Nationale de la Recherche (ANR) and Deutsche Forschungsgemeinschaft (DFG) for supporting the present research in the frame of project REGAL-ORC, grant n° ANR-20-CE92-0019.